Improved Interface of Niobium Superconducting Resonator with Ruthenium as a Capping Layer

Senthil Kumar Karuppannan,[†] Ding Huang,[‡] Naga Manikanta Kommanaboina,[†] Kamma Anil,[†] Guangxu Yan,[†] Durga Venkata Maheswar Repaka,[¶] Yiyu Zhang,[‡] Kuan Eng Johnson Goh,[∥⊥‡] Wong Seng Kai,[†] Nelson Lim Chee Beng,[†] Yap Lee Koon Sherry,[†] and Manas Mukherjee*[†#]

[†]NQFF, Institute of Materials Research and Engineering (IMRE), Agency for Science, Technology and Research (A*STAR), 2 Fusionopolis Way, Innovis Building #08-03, Singapore 138634, Republic of Singapore.

[‡]Institute of Materials Research and Engineering (IMRE), Agency for Science, Technology and Research (A*STAR), 2 Fusionopolis Way, Innovis Building #08-03, Singapore 138634, Republic of Singapore.

[¶]Electronic Materials, Institute of Materials Research and Engineering, Agency for Science, Technology and Research (A*STAR), 2 Fusionopolis Way, Innovis Building, Singapore 138634, Republic of Singapore.

[∥]Division of Physics and Applied Physics, School of Physical and Mathematical Sciences, Nanyang Technological University, Singapore, 639798 Singapore.

[⊥]Department of Physics, National University of Singapore, 2 Science Drive 3, Singapore, 117551 Singapore.

[#]Centre for Quantum Technologies, National University Singapore, Singapore, 117543, Singapore.

Corresponding author*

E-mail: Senthil_Karuppannan@imre.a-star.edu.sg; manas_mukherjee@imre.a-star.edu.sg

KEYWORDS: Ruthenium, capping layer, Resonator, internal quality factor, two-level system loss.

ABSTRACT. The current performance of superconducting circuit-based quantum processors is limited by the poor understanding of interface physics, including native surface oxide formation on the superconducting metal, which causes two-level system (TLS) loss. Niobium, a superconducting metal with a high energy gap, is an ideal choice for superconducting processors, but unfortunately, it is marred by TLS. Several methods have been proposed to minimize surface oxide on the Nb film, and considerable improvement in TLS loss has been demonstrated. These methods include surface passivation through metal capping, self-assembly of organic molecules, and post-cleaning processes. Among these, metal capping is a suitable choice despite forming a 3-5 nm thick oxide, as self-assembly and post-treatment do not protect the Nb film surface during further fabrication. Here, we have proposed ruthenium as a capping layer, forming a self-limiting oxidation with a 0.6 nm oxide thickness and predominantly producing fewer oxide compositions while being chemically resistant for further wafer fabrication processes, thus fulfilling all the criteria of an ideal capping layer. Our investigation suggests that Ru/Nb resonators have great potential as versatile and promising tools for advancing superconducting quantum technologies and integrating quantum interconnects into qubits with minimized TLS loss.

Introduction

Quantum computing represents one of the most promising advancements in computational technology, capable of solving problems beyond the reach of classical computers.[1–3] At the core of quantum computers lie qubits,[4] which utilize quantum mechanical phenomena to perform operations.[5] Superconducting qubits, in particular, have emerged as a leading platform for quantum computing due to their scalability and compatibility with existing semiconductor technologies. These circuits, made of superconducting metals with large energy gaps, operate at temperatures far below their critical temperature, allowing single microwave photons to be stored and manipulated without losing its coherence. A major challenge in superconducting quantum processors is minimizing system errors caused by unwanted sources of noise and dissipation, such as losses due to quasiparticles and two-level system TLS.[6,7] Therefore, it is crucial to develop fabrication techniques that can reduce microwave losses in superconducting quantum circuits.

Superconducting resonators are essential for the superconducting qubit readout and qubit-qubit coupling depending on the qubit architecture and serve as a valuable tool for studying microwave losses in qubits. The quality of these resonators is evaluated by the dimensionless parameter known as the internal quality factor (Qi). Higher quality factors for superconducting resonators imply longer qubit coherence times, allowing more complex quantum operations before decoherence occurs.[1,8] Achieving high Qi is challenged by energy losses primarily attributed to coupling with the TLS, often located in the insulating layers formed by native oxides at the superconducting metal-air interface.[9] Additionally, the substrate-air and substrate-metal interfaces also contribute to energy dissipation; however, the metal-air interface is particularly important due to the formation of TLS by native oxide defects and impurities.[10] These losses can negatively affect the Qi of resonators and qubits lifetime, which are pivotal for quantum computing and other advanced

technologies. Understanding and mitigating native oxide defect formation in superconducting films has thus become a central focus of research. Successfully overcoming this challenge is crucial for fully realizing the remarkable superconducting properties of metal films on a wafer scale, enabling practical applications within the burgeoning field of quantum information processing.

In recent years, the superconducting properties of niobium metal have had significant interest in the scientific community due to their remarkable characteristics, such as higher superconducting energy gap (2.3 - 2.9 meV)[11–13] and transition temperature ($T_C \simeq 9.3$K),[14–16] which make them highly valuable for various technological applications.[17,18] One key aspect of Nb film superconductivity is its relationship with the density of quasiparticles, which undergoes unique changes as a function of temperature. Notably, when the Nb films operate near 1.0 Kelvin (K), they exhibit minimal microwave loss associated with quasiparticles.[19] Thus, the study of the Nb films has opened new avenues for employing the extraordinary properties of superconductors in practical applications, including quantum computing, cryogenic computing, and high-performance cryogenic electronics. However, despite their immense potential, Nb films face challenges, particularly the formation of various surface oxides such as Nb_2O_5, NbO_2, NbO, and Nb_2O.[20,21] These oxides can detrimentally impact the superconducting performance of Nb films due to TLS and vertex doping, yet the literature addressing their precise composition and formation mechanisms is notably sparse.[7,9,20,22,23]

Recently, promising approaches for improving Qi of the Nb films have been demonstrated, including the use of self-assembled monolayer (SAM) of organic molecules,[24] metal capping,[25–28] and post-cleaning processes[15,29,30]. The SAMs consist of tailored organic molecules forming a single layer on the surface of the metal film, while metal capping involves depositing a

protective thin metal layer onto the superconducting metal film, and the post-cleaning process exposes the fabricated device to chemicals or N_2 plasma. Although SAMs and the post-cleaning processes improve the quality factor, they are limited by further fabrication processes and ageing, which can restore the surface native oxide composition to its original state. Thus, metal capping is a more stable and long-lasting approach to minimizing native oxide. Metal capping has been shown to protect native oxide growth on commonly used superconducting metals like Nb. Thin films of noble metals like gold (Au), platinum (Pt), or superconducting materials like titanium nitride (TiN), aluminium (Al), and tantalum (Ta) are used as a capping layer to protect the Nb surface from oxidation, significantly improving the quality factor of the Nb resonators and qubit coherence time in some cases.[8] However, it has been noted that the capping thin metal films themselves tend to form a 3-5 nm thick oxide on the surface, which introduces surface defects. Recently, it was demonstrated that depositing a 10 nm thick layer of surface oxide (Al_2O_3) via atomic layer deposition to prevent the formation of native oxide on a superconducting Nb film improved the quality factor at the Al_2O_3/Nb interface compared to a Nb film with the Nb native oxide.[31,32] However, this approach does not benefit qubit implementation in subsequent fabrication processes, and oxygen diffusion into the superconducting lattice remains an issue. The choice of the metal is crucial in order to minimize the oxidation of the Nb film by diffusion[33] or of the capping layers themselves by forming native oxide.[8] The two interfaces, Nb-capping and capping-vacuum, are equally responsible for hosting TLS. Thus, the ideal passivation metal should possess the following characteristics: i) which form of thin self-limited oxidation (<1 nm), ii) a minimal number of oxide compositions (RuO_x ($2<x\leq3$))[34] to reduce the occurrence of surface defects associated with oxide vacancies, and iii) chemically and

environmentally resistant to ensure that multiple fabrication processes do not adversely affect the surface quality.

In this work, we propose and demonstrate the effective protection of the surface oxide of the Nb film by a ruthenium (Ru) capping layer. This protection is achieved through the self-limiting oxidation nature of Ru, leading to a significant improvement in the quality factor of the Nb resonators by providing an oxide-free metal-air interface. Ruthenium, which exhibits a hexagonal close-packed structure, forms a self-limiting oxide layer of about 0.6 nm, preventing further oxygen diffusion and protecting the Nb/Ru interface. We show that capping Nb resonators with Ru improves their quality factor by about 83% in an average of six resonators. This work not only offers a novel strategy to protect niobium from oxidation but also provides many advantages, such as being chemically inert during the further fabrication process, stored for a longer time without any ageing effect, and having a very thin oxide layer that effectively connects with another wiring layers on planar superconducting qubits. In the following sections, we introduce the materials and methods of fabrication, present our results, and provide a conclusion on the effectiveness of the improved interface with Ru-capping.

Results and discussion

We have deposited a 100 nm thick crystalline Nb film with preferred out-of-plane orientation of (110) on a 4-inch silicon wafer with a resistivity of ≥5000Ω.cm using a multi-chamber physical vapor deposition (PVD) system at room temperature. Firstly, to remove the native oxide on the silicon wafer and unwanted organic contamination adsorbed or buried, the silicon wafer was exposed to a buffered oxide etching solution for 1 minute. Then, the wafer was loaded into the multi-chamber PVD system to deposit a 100 nm Nb film, after which the Nb deposited, wafer

was transferred to the Ru deposition chamber without breaking the vacuum and then deposited a thin (5 nm) layer of Ru at room temperature. During the transfer process, the chamber vacuum was maintained at 5×10^{-8} mbar. Finally, the wafer is removed from the deposition chamber and exposed to air. Hereafter, the Nb films with and without Ru capping will be denoted as native Nb and Nb/Ru, respectively. The standard photolithography and dry etching process were used to define the resonator structure see schematics shown in Figure 1(A-B) (see more details in supporting information). We over-etch the silicon substrate by around 100 nm to ensure the Nb film is properly etched. The over-etching depth is consistent across different resonator structures fabricated on a wafer scale (see more details in following section of the paper). We characterized the deposited Nb film crystalline structure with X-ray diffraction (XRD) measurements, which confirm the existence of the (110) out-of-plane orientation (see Figure 1C). The XRD peak positions correspond to the lattice spacing, and crystallite size can be inferred from the full width at half maximum (FWHM) of the peak, where a broader FWHM indicates a smaller crystallite size. Inset (Figure 1C) shows Ru capping leads to a small peak shift and changes in the FWHM and peak position, resulting in a change in crystallite size from 22.23 nm to 19.16 nm, which suggests that Nb/Ru has a smaller lattice spacing than Nb. Additionally, this observation shows that the Ru capping leads to a change in compressive stress as compared to that present in the native Nb film. To further understand the film quality, we characterize surface morphology using tapping-mode atomic-force microscopy (AFM); the results show that the root mean square roughness of the Nb film (0.88-0.98 nm) does not change significantly; however, we observed a notable change in the pinhole depth. Figure 1D shows a histogram of the pinhole depth profile, which indicates that there is an improvement in average pinhole depth from 4.38±1.09 nm to

3.99±0.97 nm after the Ru capping; this change is due to a reduced overall peak valley height by Ru metal fill up the sharp edge of the native Nb grain boundaries.

The amorphous native oxides at the surfaces and interfaces are known to host TLSs that contribute to microwave energy losses. We investigated the chemical composition of native oxides on native Nb film with Ru and compared it with previously reported noble and other metals to evaluate the effectiveness of Ru capping in protecting the surface oxide composition. Supplementary Figure S1 shows the X-ray photoelectron spectroscopy (XPS) spectra of Nb 3*d* for native Nb with 5nm of different capping layers, such as Cu, Pt, and Ru. The lowest band of binding energies (B.E = 201.5 to 202.5 eV) is associated with metallic Nb (Nb^0), while one doublet peak with a higher binding energy region (206−211) corresponds to Nb_2O_5 (Nb^{5+}). In addition, some smaller contributions stemming from sub-oxide or interfaces between metal oxide/metal interfaces are also visible. The results reveal that Nb/Cu samples exhibit a very weak metallic signal and a dominant oxide peak intensity around 206−210 eV, indicating the presence of a thicker surface oxide. In the case of Pt capping, the Nb-oxide peak diminishes, and the Nb-metallic peak intensity increases, confirming that Pt capping partially protects the native Nb surface from oxidation. Interestingly, in the case of Ru as a capping layer, the XPS peak corresponding to the surface native oxide completely disappears, and only a metallic peak is observed, which clearly confirms that Ru capping is the most effective in protecting the surface and the interface from oxidation. To investigate the effectiveness of Ru as a capping layer, we measured the XPS Nb 3*d* signal for Nb films with different Ru thicknesses ranging from 1 nm to 10 nm (see Figure S2). The results clearly demonstrate that a 2 nm Ru capping layer effectively prevents the formation of native Nb surface oxides. Even with a 1 nm thick Ru capping layer, significant protection against surface oxide formation is observed, confirming that Ru is five

times more effective as a capping layer than Pt. We plotted the total Nb 3*d* intensity for both oxide and metallic peaks (shown in Figure S3), which further confirms that the 1 nm Ru layer provides effective protection.

Figure 1E shows the XPS spectra of native Nb and Nb/Ru, revealing a clear difference in the surface chemical composition. In the Nb 3*d* region, the spectrum of native Nb can be well-fitted with four sets of peaks using a Gaussian-Lorentzian product line shape. Similar XPS spectra reported before[35,36] for native oxide-covered Nb films, the intensity of the Nb^{5+} peaks is significantly larger than that of the Nb^{0} peaks, indicating the formation of a native oxide layer with a thickness >5 nm.[21,37] Since the analysis depth for Al Kα XPS is typically 10 nm, we can observe the metallic Nb peak beneath the native oxide layer thickness of ≤5 nm. In the case of the Nb/Ru sample, the Nb 3*d* spectrum is dominated by the Nb^{0} peaks, followed by the Ru metal peak, with the Ru-oxide component being the less prominent (0.6nm). The Nb^{0} peak shifts from 201.45 to 202.50 eV (see Figure S4) as the capping layer thickness increases, suggesting that the binding energy of the Nb metallic peak changes with the Ru capping layer due to charge redistribution. We observed a similar shift to the higher energy side for Nb/Pt and Nb/Cu, indicating that the metallic characteristics of the Nb/NbO_x interfaces differ at the bimetallic interface, likely due to similar charge redistribution. This phenomenon has been previously reported in XPS investigations of other bimetallic interfaces.[38–40] Thus, the results clearly indicate that the surface oxidation of Nb is completely suppressed by the presence of the Ru capping layer (see Figure 1E)). The O 1*s* spectra further confirm the existence of only RuO surface oxide rather than Nb-oxide composition (see Figure 1F. The XPS results confirm that a thin layer (<5 nm) of Ru capping is sufficient to protect the superconducting metal film from surface oxidation without affecting its native crystalline structure, unlike previously reported

noble metal layers such as Pt, Au, etc. Typically, a noble metal layer of around 10 nm thickness, for example, Au, is required for complete protection against surface oxidation.[8,28] As indicated above, 5 nm of Pt and Cu does not protect the Nb surface from oxidation. It is important to minimize the thickness of the capping layer in order to preserve its native superconductivity, as the surface resistance is dependent on the capping layer thickness.[26] These results attract immediate attention from the superconducting community for applications in cryogenic electronics, quantum computing, etc.

To evaluate the effectiveness of Ru surface encapsulation in reducing microwave losses, we fabricated an Nb coplanar-waveguide (CPW) structure on a silicon wafer with and without the Ru capping layer. High-resolution cross-section TEM and EDS analysis on the patterned wafers showed the formation of native Nb oxides at the metal-air interface and SiO_x at the substrate-air interface. Figure S5 shows the over-etching depth of the silicon substrate for both Nb resonators, with and without the Ru capping layer. It clearly shows that the Nb resonator without the Ru capping layer was over-etched to a depth of ~100 nm, while the Ru-capped resonator was over-etched to a depth of ~50 nm. This indicates that the superconducting line was completely etched. The variation in over-etching is likely due to the thick native oxide present on the Nb resonator film, as native oxide generally has a much higher etching rate than the pure metal. The TEM analysis reveals the existence of 5.3 nm thick amorphous oxide on native Nb film (see Figure 2A). This observation aligns with the previously reported thickness of native oxide formation on Nb thin films.[22] The case of the Nb/Ru sample shows that the amorphous oxide completely disappeared and formed crystalline Ru with a very thin layer of native oxide around 0.6 nm (see Figure 2B). In both cases, we observed around 2 nm amorphous silicon found between Nb and crystalline silicon interface, which is due to damage caused by the pre-etching process. Figure

2(C-D) shows energy-dispersive X-ray spectroscopic images of native Nb and Nb/Ru in the resonator structures. The results further confirm that Ru capping protects against surface oxidation; however, native oxide formed at the vertical edge of the resonator structure is not covered in the current work. To the best of our knowledge, this is the first-time a near-perfect surface oxide passivation on a superconducting thin film has been demonstrated with a 5 nm thick Ru capping layer. Recently, Zhou et al.[41] showed that a 3 nm thick Mg capping layer leaves a 1 nm surface oxide on the Ta surface. Bal et al.[8] demonstrated metal layer protection by depositing a 10 nm Au capping layer using TEM and EELS techniques. Here, we characterize the surface chemical composition in detail using TEM and EDS mapping, which are consistent with XPS analysis. These results clearly show that Ru capping effectively prevents surface oxidation while self-limiting its own oxide formation with less than one nanometer.

To gain a deeper understanding of the impact of Ru capping on microwave losses, we studied coplanar waveguide resonators at cryogenic temperatures for native Nb film and compared them with Ru-capping film. We observed a more than 83% reduction in the Ru-capped resonator loss tangent compared to Nb-native resonators without the capping layer. All measurements are done in a dilution refrigerator with a base temperature of 8 mK. We characterize the losses of resonators by measuring the transmission through the microwave feedline on each sample. At the resonant frequency, the line shape of the transmission dip shows both the internal losses and the coupling to the feedline. We fit the line shape to extract the internal quality factor, Q_{int}, and the corresponding loss tangent, $\delta = 1/Q_{int}$, of the resonator. Here, the loss tangent δ refers to the total loss of the resonator, regardless of the dissipation channel. In Figure 3A, we compare the transmission spectrum of a Nb/Ru resonator with that of a baseline Nb resonator. Furthermore, we characterize the losses as a function of the intracavity photon number (Figure 3B). We

observe losses decrease with increasing microwave power for both the Nb baseline resonators and the Nb/Ru resonators, indicating that the losses are from saturable TLSs. In the single- and few-photon regimes, where TLS losses dominate, we note a significant reduction in the loss tangent with Ru surface encapsulation. Furthermore, improvements in microwave losses were observed in 83% of the fabricated devices with similar designs, indicating that Ru surface encapsulation provides a robust material improvement to superconducting quantum circuits.

Since the quest for the best capping layer can only be done by direct comparison with other metals, we have investigated the metal/oxide content of the layer for different capping metals using XPS, as shown in Supplementary Figure S1. A PVD-grown Nb and sputtered Nb with copper capping show a large presence of oxide. However, Pt-capped Nb resonators show a significant presence of oxide, which is surprising given the chemical inertness of Pt. It turns out that Pt, being a fcc crystal, shows significant porosity, and the native oxide is thicker. On the contrary, Ru, being an HCP structure, has a self-limiting property that restricts oxide formation, giving Nb/Ru films the highest metallic content.

Lastly, the composition and crystal quality of the Nb film are critically important for fabricating high-Q microwave resonators. Therefore, verifying that the Ru capping does not impact any of these properties is essential. As discussed earlier, the morphological studies indicate no change in the Nb layer; however, the properties of the capped layer can only be probed by comparing its superconducting energy gap with respect to the non-capped one. The energy gap is proportional to the critical temperature and the critical magnetic fields in type II superconducting materials. Supplementary Figure S5 shows the change in T_c with and without the capping layer as well as the Residual Resistivity Ratio (RRR) of these two samples. Interestingly, the critical magnetic field behaves nearly the same, but the Tc, as expected, shifts

to a lower value even though the RRR changes only very little. This may indicate that the Ru layer has not impacted the vortex formation but has impacted the stress in the film.

Conclusion. We have demonstrated the effectiveness of metal capping in minimizing TLS loss in a superconducting resonator operating in the microwave domain. In particular, we have shown that Ruthenium is an ideal candidate for a metal capping layer as compared to Au or Pt due to its crystal structure, which is hexagon close-packed, making it almost impossible for oxygen to diffuse in, as well as its self-restricting nature of oxide formation. The cross-section TEM and EDS of the interface clearly verifies the claim as the interface between Nb-Air and Nb-Ru is devoid (within the resolution of tools) of any oxide layer as compared to ∼5 nm of native oxide when only Nb is not capped. A chemical analysis using XPS provides more conclusive evidence that Ru significantly improves the film's metallic content, which is an essential aspect of avoiding TLS. Despite all this evidence, it is important to directly verify the effect of Ru capping on microwave photon loss in a resonator. This has also been verified by low power measurement of the resonator loss, clearly concluding that Ru capping improves, in best cases, half an order of magnitude the quality factor of a resonator as compared to no capping. Therefore, we conclude that Ru's crystal structure and chemistry are best suited as a capping layer for superconducting resonators. It is also important to note that the top metal-air interface contributes only about 10% to the loss from all the metal-air interfaces, as obtained from the surface participation ratio.[42,43] Therefore, covering the sidewall would provide much higher protection with minimal effort in process modification.

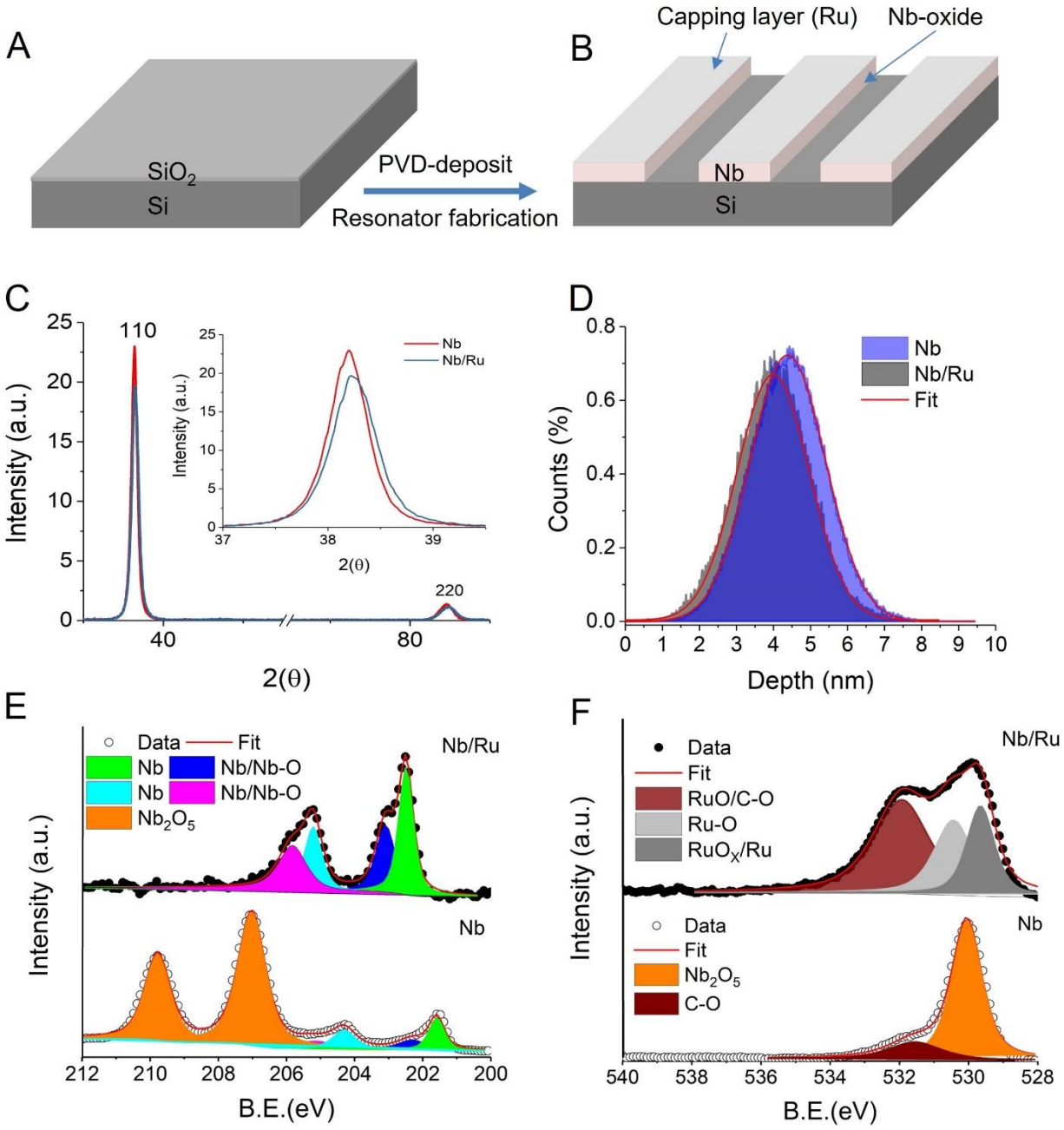

Figure 1: (A-B) Schematics of the in-situ deposition and resonator structure of Nb/Ru thin film on silicon wafer, C) X-ray diffraction (XRD) pattern of Nb thin film without and with Ru capping, insert show zoomed region of XRD single corresponding to [110] crystalline phase. D) Atomic force microscopic depth profile histogram of Nb-native and Nb/Ru thin film. E) X-ray

photoelectron spectra (XPS) of Nb 3*d* and F) XPS spectra of O 1*s* signal for Nb film Nb-native and Nb/Ru thin film.

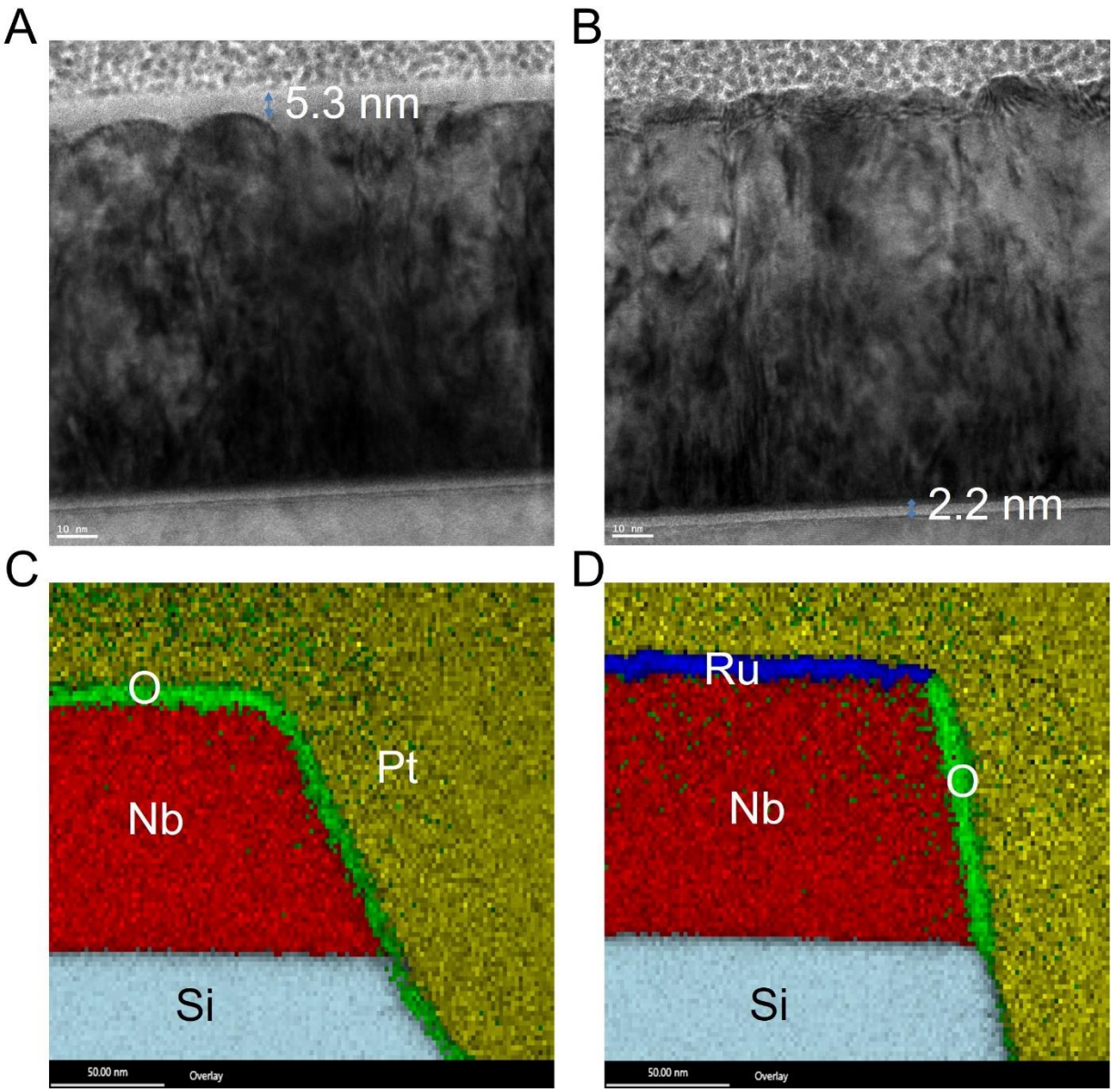

Figure 2: The bright field transmission electron microscopic images showing the cross-sectional profile of resonators after fabrication (A) native Nb film and (B) Nb/Ru. Images C and D correspond to the EDS mapping of different elements. The monolayer of oxygen content present

inside the Nb film (Fig. C-D) indicates that the lamellae were exposed to air during the transfer to TEM after cutting.

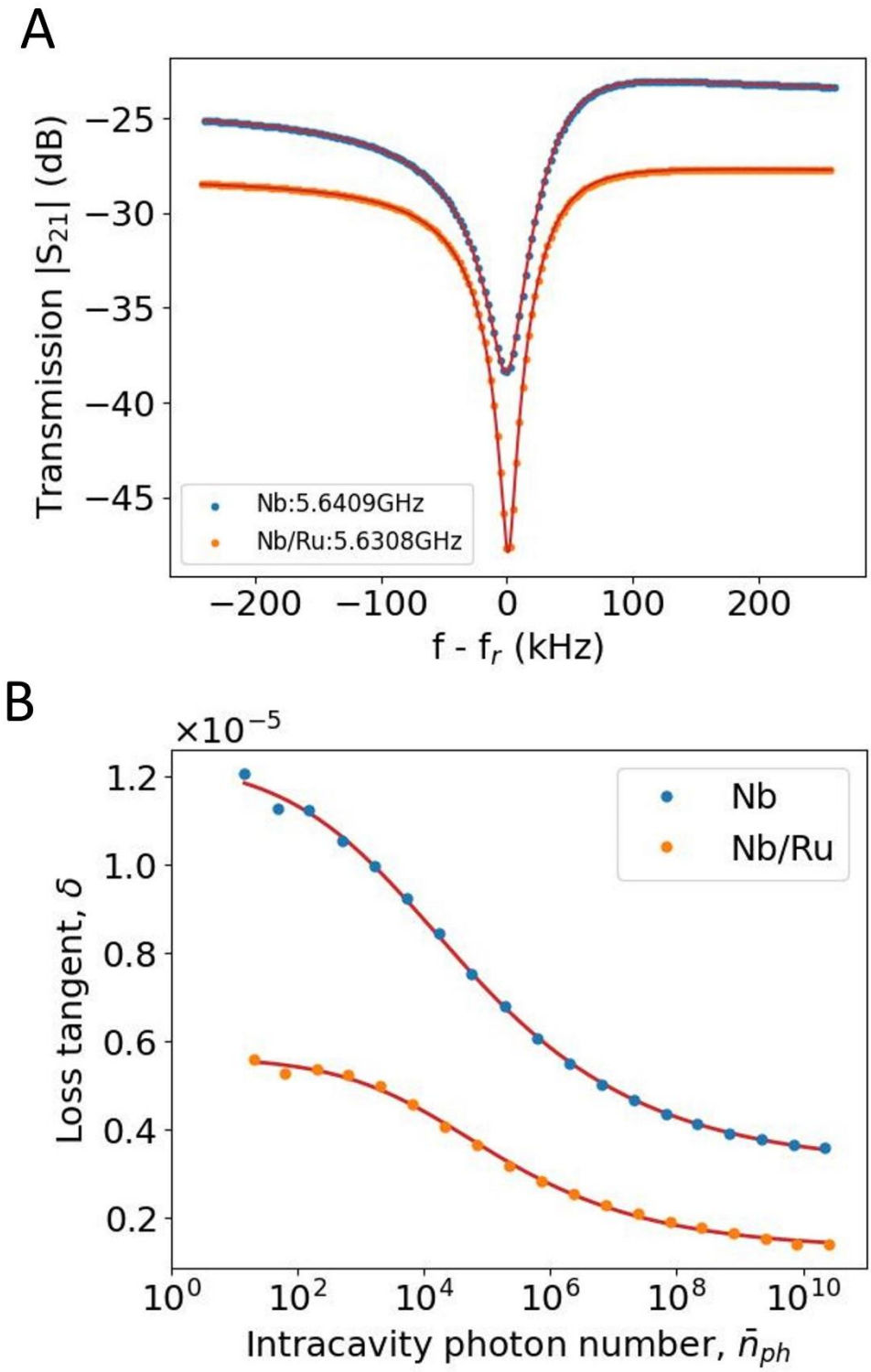

Figure 3: A) Comparison of the transmission spectra for a single Nb/Ru resonator and a Nb baseline resonator. The solid line represents a fit to the data, from which the Q_{int} and the corresponding δ are extracted.[44] B) Loss tangent of the resonators as a function of the average intracavity photon number. The solid lines represent fits to the data based on the saturation of TLSs and an additional power-independent loss.

Experimental Section

Materials

The single-side polished 4-inch Silicon (100) wafer with thickness of 550±25μm was purchased from Latech Scientific Supply Pte. Ltd. The buffered oxide etching solution (7:1 of ammonium fluoride (NH_4F) and hydrofluoric acid), developer, and other cleanroom solvents were purchased from Merck Ltd. The photoresist S1818 was purchased from MicroChemicals GmbH. The following materials were purchased and used in the TIMARIS cluster tool: Nb-ACI alloy (99.95% purity), Ru (99.95% purity, Heraeus), Pt (99.95% purity, Materion), and Cu (99.99% purity, Materion).

Thin film deposition

The multi-chamber physical vapor deposition (PVD), TIMARIS cluster tool was used to deposit 100 nm of Nb and a 5 nm Ru capping layer. First, the Silicon wafer was cleaned for 60 seconds in a buffered hydrofluoric acid solution with a ratio of 7:1 of ammonium fluoride (NH_4F) and hydrofluoric acid, followed by washing with deionized water to remove contaminants and native oxides from the Silicon surface. The wafer was then loaded into the PVD system with a process chamber base pressure of ≥5×10^{-8} Torr within 20 minutes after the cleaning process. A 100 nm thick layer of Nb metal was deposited using the TIMARIS cluster tool – a vacuum nano deposition system – with a source power of 1.4 kW, chamber pressure of 0.003335 mbar, gas flow rate of 400

sccm of Argon, substrate temperature maintained at 25° C, and a deposition rate of 10 nm/min. Before the Nb deposition, an in-situ Argon plasma cleaning was performed on the substrate in a separate etching chamber. To deposit the 5 nm Ru capping layer, the wafer with the deposited Nb was transferred to the Ru deposition chamber without breaking the vacuum. The main chamber vacuum was maintained at ≥5×10^{-8} Torr during this process. The Ru deposition was carried out with a source power of 0.8 kW, chamber pressure of 0.003335 mbar, gas flow rate of 300 sccm of Argon, and substrate temperature maintained at 25° C. For the 5 nm of Pt deposition, the DC sputtering power was set at 0.075 kW, with 400 sccm of Argon, and 10 passes were made at a speed of 51.7 mm/s. The 5 nm of Cu deposition was performed at 1.5 kW, with 300 sccm of Argon, and 1 pass was made at a speed of 163.5 mm/s. Both depositions were conducted at room temperature.

Photolithography

The resonator structure on the Nb layer is developed by optical photolithography, followed by a dry etching process. We spin-coat a positive photoresist (S1818) from ©MicroChem to define the co-planar waveguide (CPW) patterns using an MA6 mask aligner. After exposure, the resist is developed using MF-319 developer and gently rinsed with deionized water. Finally, the rinsed wafer is dried using a flow of dry N_2 gas.

Etching

The dry etching of the Nb thin film with and without a 5 nm Ru capping layer was performed using an Oxford Instruments Plasmalab100 Cobra ICP-RIE system. A 13.56 MHz power generator was connected to a copper coil to generate the ICP, and another 13.56 MHz power generator was attached to the substrate electrode to generate the DC-bias voltage. The substrate temperature was maintained at 10° C using a water-cooling system. The process chamber was pumped down to base

pressure with a turbo-molecular pump. The Ru capping layer is etched using Cl_2/O_2 etching gas at the % gas flow ratio of $Cl_2/(Cl_2+O_2)$ at 28.5% and etching conditions of RF-ICP power, RF Bias power, and process pressure at 1000W, 100W, and 10mTorr, respectively. The Nb thin films were etched using CF_4 etching gas, with etching conditions of RF ICP power, RF Bias power, and process pressure at 850W, 100W, and 5mTorr, respectively. Etching rates were measured using a surface profiler (KLA-Tencor P16).

Magnetic field-dependent transition temperature

We utilized the Physical Property Measurement System (PPMS) from Quantum Design (QD) for our temperature- and field-dependent magnetic measurements at low temperatures. We utilized the Physical Property Measurement System (PPMS) from Quantum Design (QD), USA for our temperature and field-dependent magnetic measurements at low temperatures (VSM) option. We used a sample size of 1.3 x 10.0 mm for the measurement and applied the magnetic field parallel to the film surface.

TEM characterization

We used native Nb and Nb/Ru resonators to prepare Lamellae samples, which were prepared with a FEI Helios 600 dual-beam focused-ion-beam. The primary Ga^+ ion beam was operated at 30 kV, and the final sample was cleaned at 5 kV. The final lamellae thickness was less than 100 nm. Prior to cutting, samples were coated with carbon and gold to reduce the charging effect. For TEM imaging, we use a 200 kV FEI Tecnai G2 F20 X-Twin system equipped with an EDAX Octane Elite TW55 EDS detector with a detection angle of 0.9 srad.

Critical temperature measurement

The critical temperature of the Nb film with and without the Ru capping layer was measured using a cryostat from Oxford Instruments (DRY ICE 1.0 K). Python program was used

to operate the source meter (Keithley, model 2450) to record the $I(V)$ curves by sweeping DC from +100 μA to -100 μA with a step size of 10 μA. The resistance as a function of temperature was determined by fitting the $I(V)$ curve. The resistance of the patterned conductor was continuously monitored on a temperature sweep from 1 to 10 K with a step size of 0.1 K. The critical temperature was identified by observing a sharp jump in resistance, as shown in Supplementary Figure S2A.

CPW Resonator Design

The Nb/Ru resonator geometries are the same as those of Nb resonators. In each chip, six λ_2-wave resonators are capacitively coupled to the feedline in the hanger mode geometry (trench depth up to 100 nm). All the resonators have the same centrepin width of 22 μm and gap width of 11 μm. Their lengths were swept for frequency multiplexing from 4 – 6 GHz. We estimate that the surface participation ratios and the energy participation ratio of the substrate are the same across all six resonators on the same chip. This is chosen to provide us with more statistics about the effects of Ru capping.

Resonator Measurement Setup

All devices were measured using a vector network analyzer (Keysight ENA E5080B) in a dilution refrigerator (Bluefors, BF-LD400) with a ~ 8 mK base temperature at the mixing chamber plate. The input line of the microwave signal was attenuated at different stages (20 dB at the 4 K plate, 20 dB at the cold plate, 20 dB at the mixing chamber plate) using cryogenic attenuators (XMA Corporation, 2682-6460-20-CRYO Bulk) with a total attenuation of 60 dB. After attenuation, the microwave signal was filtered using a bandpass filter (Keenlion, KBF-4/8-2S) and an IR filter (Bluefors IR filter). The total input line attenuation across the lines is around 69 dB at resonator frequencies. On the output line, the signal was isolated with three isolators, two from

QuinStar Technology (QCI-G0400801AS) and one from Low Noise Factory (LNF-ISISISC4 _8A), and filtered with a bandpass filter (Keenlion, KBF-4/8-2S) and an IR filter (Bluefors IR filter). After isolation and filtering, the signal was amplified with a HEMT amplifier (Low Noise Factory, LNF-LNC4 _8F) at the 4 K stage followed by a room temperature amplifier (Mini-Circuits, ZVA-183-S+) outside the dilution refrigerator. The samples were packaged in a QCage.[24,44] magnetic shielding and the accompanying sample holder.

Data Analysis for Resonator Measurements:

We probe the resonator quality factors by measuring the transmission through the feedline on each sample. We fit the S21 traces following the method presented in Ref[45], with the equation (1)

$$S_{21} = A\left(1 + \alpha\frac{f - f_r}{f_r}\right)\left(1 - \frac{\frac{Q_l}{|Q_e|}e^{i\theta}}{1 + 2iQ_l\frac{f - f_r}{f_r}}\right)e^{i(\phi_v f + \phi_0)} \quad (1)$$

where A is the transmission amplitude away from the resonance, Q_l is the loaded quality factor of the resonator, Q_e is the external quality factor, f_r is the center frequency of the resonance. The fitted Q_i and Q_c are extracted using $1/Q_l = 1/Q_c + 1/Q_i$ and $1/Q_c = Re(1/Q_e)$. This fitting procedure allows us to get both the Q_c and the Q_i. The fitted Q_c is within a factor of 5 from our design.

Supporting Information Available

The following files are available free of charge. Figure S1: XPS spectra of Nb 3d peak for native Nb and with different metal capping layer (all metal capping layer thickness ≃5nm), and Figure S2 The superconducting transition temperature of Nb and Nb/Ru films, and B) the superconducting transition temperature as a function of a magnetic field.

AUTHOR INFORMATION

Corresponding Authors

karuppannansk@imre.a-star.edu.sg and manas_mukherjee@imre.a-star.edu.sg

Author contributions

The manuscript was written with the contributions of all authors, and all authors have approved the final version.

Acknowledgment

This research is supported by the National Research Foundation, Singapore and A*STAR under its Quantum Engineering Programme (NRF2021-QEP2-03-P07/W21Qpd0307) and A*star SRP (C222517002). D.H. acknowledges funding support from A*STAR project C222812022 and MTC YIRG M22K3c0105. SKK would like to acknowledge Debbie SENG Hwee Leng from Advanced Characterization and Instrumentation, IMRE, A*STAR, Singapore for XPS characterization.

References

(1) Bravyi, S.; Dial, O.; Gambetta, J. M.; Gil, D.; Nazario, Z. The Future of Quantum Computing with Superconducting Qubits. *J. Appl. Phys.* **2022**, *132* (16), 160902. https://doi.org/10.1063/5.0082975.

(2) Tindall, J.; Fishman, M.; Stoudenmire, E. M.; Sels, D. Efficient Tensor Network Simulation of IBM's Eagle Kicked Ising Experiment. *PRX Quantum* **2024**, *5* (1), 010308. https://doi.org/10.1103/PRXQuantum.5.010308.

(3) Arute, F.; Arya, K.; Babbush, R.; Bacon, D.; Bardin, J. C.; Barends, R.; Biswas, R.; Boixo,

S.; Brandao, F. G. S. L.; Buell, D. A.; Burkett, B.; Chen, Y.; Chen, Z.; Chiaro, B.; Collins, R.; Courtney, W.; Dunsworth, A.; Farhi, E.; Foxen, B.; Fowler, A.; Gidney, C.; Giustina, M.; Graff, R.; Guerin, K.; Habegger, S.; Harrigan, M. P.; Hartmann, M. J.; Ho, A.; Hoffmann, M.; Huang, T.; Humble, T. S.; Isakov, S. V.; Jeffrey, E.; Jiang, Z.; Kafri, D.; Kechedzhi, K.; Kelly, J.; Klimov, P. V.; Knysh, S.; Korotkov, A.; Kostritsa, F.; Landhuis, D.; Lindmark, M.; Lucero, E.; Lyakh, D.; Mandrà, S.; McClean, J. R.; McEwen, M.; Megrant, A.; Mi, X.; Michielsen, K.; Mohseni, M.; Mutus, J.; Naaman, O.; Neeley, M.; Neill, C.; Niu, M. Y.; Ostby, E.; Petukhov, A.; Platt, J. C.; Quintana, C.; Rieffel, E. G.; Roushan, P.; Rubin, N. C.; Sank, D.; Satzinger, K. J.; Smelyanskiy, V.; Sung, K. J.; Trevithick, M. D.; Vainsencher, A.; Villalonga, B.; White, T.; Yao, Z. J.; Yeh, P.; Zalcman, A.; Neven, H.; Martinis, J. M. Quantum Supremacy Using a Programmable Superconducting Processor. *Nature* **2019**, *574* (7779), 505–510. https://doi.org/10.1038/s41586-019-1666-5.

(4) Clarke, J.; Wilhelm, F. K. Superconducting Quantum Bits. *Nature* **2008**, *453* (7198), 1031–1042. https://doi.org/10.1038/nature07128.

(5) Gambetta, J. M.; Chow, J. M.; Steffen, M. Building Logical Qubits in a Superconducting Quantum Computing System. *npj Quantum Inf.* **2017**, *3* (1), 2. https://doi.org/10.1038/s41534-016-0004-0.

(6) Murray, C. E. Material Matters in Superconducting Qubits. *Mater. Sci. Eng. R Reports* **2021**, *146*, 100646. https://doi.org/10.1016/j.mser.2021.100646.

(7) McRae, C. R. H.; Wang, H.; Gao, J.; Vissers, M. R.; Brecht, T.; Dunsworth, A.; Pappas, D. P.; Mutus, J. Materials Loss Measurements Using Superconducting Microwave Resonators.

Rev. Sci. Instrum. **2020**, *91* (9), 091101. https://doi.org/10.1063/5.0017378.

(8) Bal, M.; Murthy, A. A.; Zhu, S.; Crisa, F.; You, X.; Huang, Z.; Roy, T.; Lee, J.; Zanten, D. van; Pilipenko, R.; Nekrashevich, I.; Lunin, A.; Bafia, D.; Krasnikova, Y.; Kopas, C. J.; Lachman, E. O.; Miller, D.; Mutus, J. Y.; Reagor, M. J.; Cansizoglu, H.; Marshall, J.; Pappas, D. P.; Vu, K.; Yadavalli, K.; Oh, J.-S.; Zhou, L.; Kramer, M. J.; Lecocq, F.; Goronzy, D. P.; Torres-Castanedo, C. G.; Pritchard, P. G.; Dravid, V. P.; Rondinelli, J. M.; Bedzyk, M. J.; Hersam, M. C.; Zasadzinski, J.; Koch, J.; Sauls, J. A.; Romanenko, A.; Grassellino, A. Systematic Improvements in Transmon Qubit Coherence Enabled by Niobium Surface Encapsulation. *npj Quantum Inf.* **2024**, *10* (1), 43. https://doi.org/10.1038/s41534-024-00840-x.

(9) Burnett, J.; Faoro, L.; Lindström, T. Analysis of High Quality Superconducting Resonators: Consequences for TLS Properties in Amorphous Oxides. *Supercond. Sci. Technol.* **2016**, *29* (4), 044008. https://doi.org/10.1088/0953-2048/29/4/044008.

(10) Drimmer, M.; Telkamp, S.; Fischer, F. L.; Rodrigues, I. C.; Todt, C.; Krizek, F.; Kriegner, D.; Müller, C.; Wegscheider, W.; Chu, Y. The Effect of Niobium Thin Film Structure on Losses in Superconducting Circuits. **2024**, 1-18. http://arxiv.org/abs/2403.12164.

(11) Bonnet, D.; Erlenkämper, S.; Germer, H.; Rabenhorst, H. A New Measurement of the Energy Gap in Superconducting Niobium. *Phys. Lett. A* **1967**, *25* (6), 452–453. https://doi.org/10.1016/0375-9601(67)90076-X.

(12) Pronin, A. V.; Dressel, M.; Pimenov, A.; Loidl, A.; Roshchin, I. V.; Greene, L. H. Direct Observation of the Superconducting Energy Gap Developing in the Conductivity Spectra of Niobium. *Phys. Rev. B* **1998**, *57* (22), 14416–14421.

https://doi.org/10.1103/PhysRevB.57.14416.

(13) Lee, J.; Sung, Z.; Murthy, A. A.; Grassellino, A.; Romanenko, A.; Sitaraman, N. S.; Arias, T. A. Stress-Induced Structural Changes in Superconducting Nb Thin Films. *Phys. Rev. Mater.* **2023**, *7* (6), 1-7. https://doi.org/10.1103/PhysRevMaterials.7.L063201.

(14) Kittiwatanakul, S.; Anuniwat, N.; Dao, N.; Wolf, S. A.; Lu, J. Surface Morphology Control of Nb Thin Films by Biased Target Ion Beam Deposition. *J. Vac. Sci. Technol. A Vacuum, Surfaces, Film.* **2018**, *36* (3), 031507. https://doi.org/10.1116/1.5023723.

(15) Kowsari, D.; Zheng, K.; Monroe, J. T.; Thobaben, N. J.; Du, X.; Harrington, P. M.; Henriksen, E. A.; Wisbey, D. S.; Murch, K. W. Fabrication and Surface Treatment of Electron-Beam Evaporated Niobium for Low-Loss Coplanar Waveguide Resonators. *Appl. Phys. Lett.* **2021**, *119* (13), 132601. https://doi.org/10.1063/5.0066441.

(16) Katzir, E.; Yochelis, S.; Zeides, F.; Katz, N.; Kalcheim, Y.; Millo, O.; Leitus, G.; Myasodeyov, Y.; Shapiro, B. Y.; Naaman, R.; Paltiel, Y. Increased Superconducting Transition Temperature of a Niobium Thin Film Proximity Coupled to Gold Nanoparticles Using Linking Organic Molecules. *Phys. Rev. Lett.* **2012**, *108* (10), 107004. https://doi.org/10.1103/PhysRevLett.108.107004.

(17) Kar, S.; Weiland, C.; Zhou, C.; Bhatia, E.; Martinick, B.; Nalaskowski, J.; Mucci, J.; Olson, S.; Hung, P. Y.; Wells, I.; Frost, H.; Johnson, C. S.; Murray, T.; Kaushik, V.; Kirkpatrick, S.; Chau, K.; Walsh, M. J.; Liu, M.; Papa Rao, S. S. Engineering of Niobium Surfaces through Accelerated Neutral Atom Beam Technology for Quantum Applications. *J. Appl. Phys.* **2023**, *134* (2), 025301. https://doi.org/10.1063/5.0153617.

(18) Ries, R.; Seiler, E.; Gömöry, F.; Medvids, A.; Pira, C.; Malyshev, O. B. Superconducting Properties and Surface Roughness of Thin Nb Samples Fabricated for SRF Applications. *J. Phys. Conf. Ser.* **2020**, *1559* (1), 012040. https://doi.org/10.1088/1742-6596/1559/1/012040.

(19) Leo, A.; Grimaldi, G.; Citro, R.; Nigro, A.; Pace, S.; Huebener, R. P. Quasiparticle Scattering Time in Niobium Superconducting Films. *Phys. Rev. B* **2011**, *84* (1), 014536. https://doi.org/10.1103/PhysRevB.84.014536.

(20) Premkumar, A.; Weiland, C.; Hwang, S.; Jäck, B.; Place, A. P. M.; Waluyo, I.; Hunt, A.; Bisogni, V.; Pelliciari, J.; Barbour, A.; Miller, M. S.; Russo, P.; Camino, F.; Kisslinger, K.; Tong, X.; Hybertsen, M. S.; Houck, A. A.; Jarrige, I. Microscopic Relaxation Channels in Materials for Superconducting Qubits. *Commun. Mater.* **2021**, *2* (1), 72. https://doi.org/10.1038/s43246-021-00174-7.

(21) Wenskat, M.; Čižek, J.; Liedke, M. O.; Butterling, M.; Stiehl, M.; Semione, G. D. L.; Backes, C.; Bate, C.; Melikhova, O.; Hirschmann, E.; Wagner, A.; Weise, H.; Stierle, A.; Aeschlimann, M.; Hillert, W. Vacancy Dynamics in Niobium and Its Native Oxides and Their Potential Implications for Quantum Computing and Superconducting Accelerators. *Phys. Rev. B* **2022**, *106* (9), 094516. https://doi.org/10.1103/PhysRevB.106.094516.

(22) Verjauw, J.; Potočnik, A.; Mongillo, M.; Acharya, R.; Mohiyaddin, F.; Simion, G.; Pacco, A.; Ivanov, T.; Wan, D.; Vanleenhove, A.; Souriau, L.; Jussot, J.; Thiam, A.; Swerts, J.; Piao, X.; Couet, S.; Heyns, M.; Govoreanu, B.; Radu, I. Investigation of Microwave Loss Induced by Oxide Regrowth in High- Q Niobium Resonators. *Phys. Rev. Appl.* **2021**, *16* (1), 1–14. https://doi.org/10.1103/PhysRevApplied.16.014018.

(23) Breeze, J. D.; Perkins, J. M.; McComb, D. W.; Alford, N. M. N. Do Grain Boundaries Affect Microwave Dielectric Loss in Oxides? *J. Am. Ceram. Soc.* **2009**, *92* (3), 671–674. https://doi.org/10.1111/j.1551-2916.2009.02932.x.

(24) Alghadeer, M.; Banerjee, A.; Hajr, A.; Hussein, H.; Fariborzi, H.; Rao, S. G. Surface Passivation of Niobium Superconducting Quantum Circuits Using Self-Assembled Monolayers. *ACS Appl. Mater. Interfaces* **2023**, *15* (1), 2319–2328. https://doi.org/10.1021/acsami.2c15667.

(25) Flokstra, M.; Stewart, R.; Yim, C. M.; Trainer, C.; Wahl, P.; Miller, D.; Satchell, N.; Burnell, G.; Luetkens, H.; Prokscha, T.; Suter, A.; Morenzoni, E.; Bobkova, I. V.; Bobkov, A. M.; Lee, S. Spin-Orbit Driven Superconducting Proximity Effects in Pt/Nb Thin Films. *Nat. Commun.* **2023**, *14* (1), 5081. https://doi.org/10.1038/s41467-023-40757-1.

(26) Oseroff, T.; Sun, Z.; Liepe, M. U. Measurements of the Amplitude-Dependent Microwave Surface Resistance of an Au/Nb Bilayer. *Supercond. Sci. Technol.* **2023**, *36* (11), 115009. https://doi.org/10.1088/1361-6668/acf88d.

(27) Blatter, G.; Sirena, M.; Haberkorn, N. Enhancement of the Vortex Critical Velocity in Superconducting/Normal Metal Bilayers. *Mater. Sci. Eng. B* **2024**, 299, 116943. https://doi.org/10.1016/j.mseb.2023.116943.

(28) de Ory, M. C.; Rodriguez, D.; Magaz, M. T.; Rollano, V.; Granados, D.; Gomez, A. Low Loss Hybrid Nb/Au Superconducting Resonators for Quantum Circuit Applications. **2024**, 1–7.

(29) Mergenthaler, M.; Müller, C.; Ganzhorn, M.; Paredes, S.; Müller, P.; Salis, G.; Adiga, V.

P.; Brink, M.; Sandberg, M.; Hertzberg, J. B.; Filipp, S.; Fuhrer, A. Effects of Surface Treatments on Flux Tunable Transmon Qubits. *npj Quantum Inf.* **2021**, *7* (1), 157. https://doi.org/10.1038/s41534-021-00491-2.

(30) Zheng, K.; Kowsari, D.; Thobaben, N. J.; Du, X.; Song, X.; Ran, S.; Henriksen, E. A.; Wisbey, D. S.; Murch, K. W. Nitrogen Plasma Passivated Niobium Resonators for Superconducting Quantum Circuits. *Appl. Phys. Lett.* **2022**, *120* (10), 102601. https://doi.org/10.1063/5.0082755.

(31) Wenskat, M.; Deyu, G. K.; González Díaz-Palacio, I.; Blick, R. H.; Zierold, R.; Hillert, W. Successful Al2O3 Coating of Superconducting Niobium Cavities with Thermal ALD. *Supercond. Sci. Technol.* **2023**, *36* (1), 015010. https://doi.org/10.1088/1361-6668/aca83f.

(32) Kalboussi, Y.; Delatte, B.; Bira, S.; Dembele, K.; Li, X.; Miserque, F.; Brun, N.; Walls, M.; Maurice, J. L.; Dragoe, D.; Leroy, J.; Longuevergne, D.; Gentils, A.; Jublot-Leclerc, S.; Jullien, G.; Eozenou, F.; Baudrier, M.; Maurice, L.; Proslier, T. Reducing Two-Level Systems Dissipations in 3D Superconducting Niobium Resonators by Atomic Layer Deposition and High Temperature Heat Treatment. *Appl. Phys. Lett.* **2024**, *124* (13), 134001. https://doi.org/10.1063/5.0202214.

(33) Zafar, S.; Jagannathan, H.; Edge, L. F.; Gupta, D. Measurement of Oxygen Diffusion in Nanometer Scale HfO2 Gate Dielectric Films. *Appl. Phys. Lett.* **2011**, *98* (15), 152903. https://doi.org/10.1063/1.3579256.

(34) Coloma Ribera, R.; Van De Kruijs, R. W. E.; Kokke, S.; Zoethout, E.; Yakshin, A. E.; Bijkerk, F. Surface and Sub-Surface Thermal Oxidation of Thin Ruthenium Films. *Appl. Phys. Lett.* **2014**, *105* (13), 131601. https://doi.org/10.1063/1.4896993.

(35) Prudnikava, A.; Tamashevich, Y.; Babenkov, S.; Makarova, A.; Smirnov, D.; Aristov, V.; Molodtsova, O.; Kugeler, O.; Viefhaus, J.; Foster, B. Systematic Study of Niobium Thermal Treatments for Superconducting Radio Frequency Cavities Employing X-Ray Photoelectron Spectroscopy. *Supercond. Sci. Technol.* **2022**, *35* (6), 065019. https://doi.org/10.1088/1361-6668/ac6a85.

(36) Van Damme, J.; Ivanov, T.; Favia, P.; Conard, T.; Verjauw, J.; Acharya, R.; Perez Lozano, D.; Raes, B.; Van de Vondel, J.; Vadiraj, A. M.; Mongillo, M.; Wan, D.; De Boeck, J.; Potočnik, A.; De Greve, K. Argon-Milling-Induced Decoherence Mechanisms in Superconducting Quantum Circuits. *Phys. Rev. Appl.* **2023**, *20* (1), 014034. https://doi.org/10.1103/PhysRevApplied.20.014034.

(37) Semione, G. D. L.; Pandey, A. D.; Tober, S.; Pfrommer, J.; Poulain, A.; Drnec, J.; Schütz, G.; Keller, T. F.; Noei, H.; Vonk, V.; Foster, B.; Stierle, A. Niobium Near-Surface Composition during Nitrogen Infusion Relevant for Superconducting Radio-Frequency Cavities. *Phys. Rev. Accel. Beams* **2019**, *22* (10), 103102. https://doi.org/10.1103/PhysRevAccelBeams.22.103102.

(38) Cano, A.; Eremeev, G. V.; R Zuazo, J.; Lee, J.; Luo, B.; Martinello, M.; Romanenko, A.; Posen, S. Selective Thermal Evolution of a Native Oxide Layer in Nb and Nb $_3$ Sn-Coated SRF Grade Nb: An *In Situ* XPS Study. *J. Phys. Chem. C* **2023**, *127* (39), 19705–19716. https://doi.org/10.1021/acs.jpcc.3c03108.

(39) Yang, Z.; Wu, R. First-Principles Studies on Bonding Mechanism at Ni/X Bimetallic Interfaces (X=Ta, W, Re and Ru). *Surf. Sci.* **2000**, *469* (1), 36–44. https://doi.org/10.1016/S0039-6028(00)00809-8.

(40) Riffe, D. M.; Shinn, N. D.; Kim, B.; Kim, K. J.; Kang, T.-H. Core-Level Shifts at the Pt/W(110) Monolayer Bimetallic Interface. *Surf. Sci.* **2009**, *603* (24), 3431–3438. https://doi.org/10.1016/j.susc.2009.10.006.

(41) Zhou, C.; Mun, J.; Yao, J.; Anbalagan, A. kumar; Hossain, M. D.; McLellan, R. A.; Li, R.; Kisslinger, K.; Li, G.; Tong, X.; Head, A. R.; Weiland, C.; Hulbert, S. L.; Walter, A. L.; Li, Q.; Zhu, Y.; Sushko, P. V.; Liu, M. Ultrathin Magnesium-Based Coating as an Efficient Oxygen Barrier for Superconducting Circuit Materials. *Adv. Mater.* **2024**, *36* (18), 2310280. https://doi.org/10.1002/adma.202310280.

(42) Chang, R. D.; Shumiya, N.; McLellan, R. A.; Zhang, Y.; Bland, M. P.; Bahrami, F.; Mun, J.; Zhou, C.; Kisslinger, K.; Cheng, G.; Pakpour-Tabrizi, A. C.; Yao, N.; Zhu, Y.; Liu, M.; Cava, R. J.; Gopalakrishnan, S.; Houck, A. A.; de Leon, N. P. Eliminating Surface Oxides of Superconducting Circuits with Noble Metal Encapsulation. **2024**, 1-17. https://doi.org/10.48550/arXiv.2408.13051

(43) Wenner, J.; Barends, R.; Bialczak, R. C.; Chen, Y.; Kelly, J.; Lucero, E.; Mariantoni, M.; Megrant, A.; O'Malley, P. J. J.; Sank, D.; Vainsencher, A.; Wang, H.; White, T. C.; Yin, Y.; Zhao, J.; Cleland, A. N.; Martinis, J. M. Surface Loss Simulations of Superconducting Coplanar Waveguide Resonators. *Appl. Phys. Lett.* **2011**, *99* (11), 113513. https://doi.org/10.1063/1.3637047.

(44) Probst, S.; Song, F. B.; Bushev, P. A.; Ustinov, A. V.; Weides, M. Efficient and Robust Analysis of Complex Scattering Data under Noise in Microwave Resonators. *Rev. Sci. Instrum.* **2015**, *86* (2), 024706. https://doi.org/10.1063/1.4907935.

(45) Bruno, A.; de Lange, G.; Asaad, S.; van der Enden, K. L.; Langford, N. K.; DiCarlo, L.

Reducing Intrinsic Loss in Superconducting Resonators by Surface Treatment and Deep Etching of Silicon Substrates. *Appl. Phys. Lett.* **2015**, *106* (18), 182601. https://doi.org/10.1063/1.4919761.

For Table of Contents Use Only